Application of a Quantum Cascade Laser for Time-Resolved, in Situ Probing of CH_4/H_2 and C_2H_2/H_2 Gas Mixtures during Microwave Plasma Enhanced Chemical Vapor Deposition of Diamond

A. Cheesman, J. A. Smith, and M. N. R. Ashfold*

School of Chemistry, University of Bristol, Bristol, United Kingdom BS8 1TS

N. Langford, S. Wright, and G. Duxbury

Department of Physics, University of Strathclyde, John Anderson Building, 107 Rottenrow, Glasgow, United Kingdom G4 0NG

Received: November 16, 2005; In Final Form: January 10, 2006

First illustrations of the utility of pulsed quantum cascade lasers for in situ probing of the chemistry prevailing in microwave plasma activated hydrocarbon/Ar/H_2 gas mixtures used for diamond thin film growth are reported. CH_4 and C_2H_2 molecules, and their interconversion, have been monitored by line-of-sight single pass absorption methods, as a function of process conditions (e.g., choice of input hydrocarbon (CH_4 or C_2H_2), hydrocarbon mole fraction, total gas pressure, and applied microwave power). The observed trends can be rationalized, qualitatively, within the framework of the previously reported modeling of the gas-phase chemistry prevailing in hot filament activated hydrocarbon/H_2 gas mixtures (Ashfold et al. *Phys. Chem. Chem. Phys.* **2001**, *3*, 3471). Column densities of vibrationally excited $C_2H_2(v_5=1)$ molecules at low input carbon fractions are shown to be far higher than expected on the basis of local thermodynamic equilibrium. The presence of vibrationally excited C_2H_2 molecules ($C_2H_2^{\ddagger}$) can be attributed to the exothermicity of the $C_2H_3 + H \rightleftharpoons C_2H_2 + H_2$ elementary reaction within the overall multistep $CH_4 \rightarrow C_2H_2$ conversion. Diagnostic methods that sample just $C_2H_2(v=0)$ molecules thus run the risk of underestimating total C_2H_2 column densities in hydrocarbon/H_2 mixtures operated under conditions where the production rate of $C_2H_2^{\ddagger}$ molecules exceeds their vibrational relaxation (and thermal equilibration) rates.

Introduction

Most diamond chemical vapor deposition (CVD) is brought about by using dilute methane/H_2 gas mixtures, activated by, for example, microwave (MW) or arc-jet plasmas, or the surface of a hot filament (HF). Activation leads to dissociation of molecular hydrogen, and formation of H atoms. These atoms play several important roles, the most important of which in the context of the present work is activation of gas-phase hydrocarbon species via the sequence of H-shifting reactions 1.

$$CH_y + H \rightleftharpoons CH_{y-1} + H_2 \qquad (y = 4-1) \qquad (1)$$

Self-reactions between the resulting CH_{y-1} radicals can yield C_2H_x ($x \leq 6$) species, which participate in a similar sequence of H-shifting reactions 2.

$$C_2H_x + H \rightleftharpoons C_2H_{x-1} + H_2 \qquad (x = 6-1) \qquad (2)$$

Any thorough understanding of the diamond CVD process thus requires rather detailed knowledge of the chemical environment immediately adjacent to the growing film surface. References 1−3 review many of the pioneering efforts to probe such environments, and begin unravelling details of the chemical transformations occurring in the gas phase and at the gas−surface interface. Techniques that have been used to shed light on such issues span optical emission spectroscopy, in situ mass spectrometry,[4,5] and a number of laser spectroscopy methods. Included among the latter are the pioneering infrared (IR) diode laser absorption studies of stable hydrocarbons and hydrocarbon radicals (e.g., C_2H_2, C_2H_4, and CH_3) by Butler's group[1,6] and the widespread use of visible and near-ultraviolet dye lasers to probe radical species such as CH and C_2 by laser induced fluorescence,[7] CH_3,[8,9] CH, and C_2[10,11] by cavity enhanced absorption methods, and H atoms[12−14] and CH_3 radicals[15] by multiphoton excitation methods. Such data would, ideally, consist of spatially resolved absolute number densities, measured as a function of process conditions. In practice, only absorption methods are well-suited to absolute concentration measurements, and the densities returned are normally line-of-sight column densities. Without very careful calibration studies, the other methods will generally only provide relative concentrations. These data, taken in conjunction with complementary two- (2-D) or three-dimensional (3-D) reactor modeling,[16,17] are largely responsible for the current level of understanding of the gas-phase chemistry underpinning diamond CVD.[2,3]

A key feature of this understanding is the recognition of high H atom number densities throughout the reactor—even in the peripheral, cooler regions, where the H atom densities far exceed those expected on the basis of local thermodynamic equilibrium. This reflects the paucity of efficient H atom loss processes in these gas mixtures (which typically contain 95−99% H_2). These H atoms not only drive the families of radical forming H shifting abstraction reactions 1 and 2 but also, in the cooler regions,

* Address correspondence to this author. Phone: 117-928-8312 or 117-928-8313. Fax: 117-925-0612. E-mail: mike.ashfold@bris.ac.uk.

10.1021/jp056622u CCC: $33.50
Published on Web 02/08/2006

participate in H addition reactions that convert C_2H_2 (the most stable C_2H_x species at high gas temperatures) back to the CH_y family.[3,16] If the $CH_y \rightleftharpoons C_2H_x$ interconversions are sufficiently rapid, it follows that the detailed distribution of CH_y, C_2H_x, etc. species present in an activated hydrocarbon/H_2 gas mixture should be relatively insensitive to the precise choice of hydrocarbon feedstock gas. In support of this view, a number of early diamond film growth studies demonstrated that similar morphologies and growth rates could indeed be obtained by using different hydrocarbon source gases (at a constant input carbon mole fraction).[18]

While qualitatively correct, there is a wealth of available data to suggest that this assumption cannot be correct in detail. For example, our earlier comparison of HF activated 1% CH_4/H_2 and 0.5% C_2H_2/H_2 gas mixtures indicated $\sim 3\times$ higher near-filament CH_3 radical number densities in the former.[15] There remains a continuing need for new and improved, nonintrusive, in situ probes of the gas-phase chemistry and composition—not just to quantify such differences better and to move our understanding of the diamond CVD process to a higher level, but also from the viewpoint of improved process control. Here we provide first illustrations of the potential of quantum cascade (QC) laser technology[19−21] to address some of these issues. Specifically, we have employed a pulsed QC laser operating at ~ 1275 cm^{-1} to probe CH_4 and C_2H_2 molecules, and their interconversion, in a 1.5 kW MW reactor operating with both $CH_4/Ar/H_2$ and $C_2H_2/Ar/H_2$ gas mixtures, as a function of process conditions (e.g., input hydrocarbon mole fraction, total gas pressure, and applied MW power). In addition, the rapid sweep rate of such pulsed QC lasers has enabled new insights into the time evolution of the CH_4/C_2H_2 ratio when either is introduced into (or removed from) an established Ar/H_2 plasma.

Experimental Section

The plasma of interest was maintained in a custom designed and built MW reactor (2 kW, 2.45 GHz Muegge power supply and generator) operating with mixtures of hydrocarbon (CH_4 or C_2H_2), Ar, and H_2 (BOC, with respective stated purities of 99.5% (CH_4), 98.5% (C_2H_2), 99.995% (Ar), and 99.995% (H_2)). The reactor has the general form of a vertically aligned cylinder of volume ~ 600 cm^3, with MW power fed from above through a quartz window. The respective gas flows are metered through individual mass flow controllers (MFCs) and premixed prior to introduction into the reactor through two 6.25 mm diameter stainless steel inlet pipes located near the top, and on opposite sides, of the reactor. The chamber is exhausted through six, radially symmetric, 6.25 mm diameter pumping ports machined into its base, using a two-stage rotary pump (Edwards E2M8). An in-line feedback controlled throttle valve between the reactor and this pump enables stable operation at any user-specified pressure in the range $40 \leq P \leq 200$ Torr. Diamond is deposited (at growth rates of ~ 2 μm h^{-1} under standard operating conditions) on a pre-abraded, polished Mo substrate (30 mm diameter) mounted centrally on the (detachable) water-cooled base of the reactor. The substrate temperature is monitored by a single color optical pyrometer. The column probed by the laser is defined by two 4 mm diameter apertures mounted on opposite sides of the reactor, allowing single-pass line-of-sight monitoring along an axis parallel to, and 13 mm above, the substrate surface. In the present experiments, these apertures were sealed by thin, polished CVD diamond windows (Element Six Ltd) mounted on wedged flanges so as to minimize etaloning effects. The window−window separation, and thus the length of the sampled column, was $l = 19.0$ cm, of which the luminous plasma ball appeared to span the central ~ 30 mm.

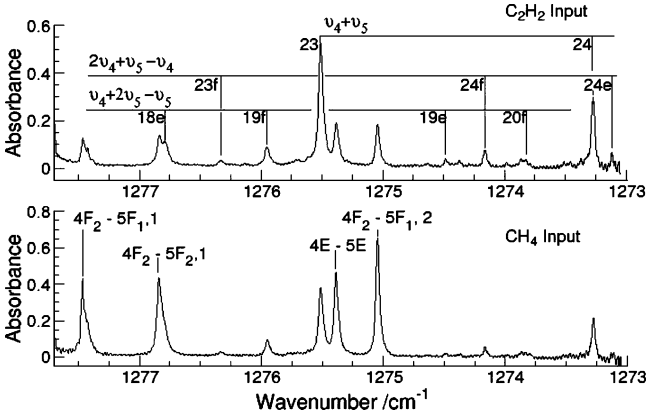

Figure 1. Line-of-sight absorption spectra of MW activated 4.4% C_2H_2/7% Ar/H_2 (upper panel) and 8.8% CH_4/7% Ar/H_2 gas mixtures. The carbon fraction, the total flow rate (565 sccm), total pressure (150 Torr), and applied MW power (1.5 kW) are the same in both cases. C_2H_2 and CH_4 absorptions are present in both spectra, with different relative intensities. Features due to C_2H_2 and to CH_4 are indicated in the upper and lower panels, respectively. Details of these assignments are given in Table 1.

The QC laser spectrometer, and its operation, have been described elsewhere.[21−23] The present experiments employed an 8 μm laser, mounted in a compact QC laser head and driver developed by Cascade Technologies Ltd.[24] When operating at -2 °C, the output wavenumber from the laser could be swept from 1277.6 to 1273.0 cm^{-1} (a 140 GHz tuning range) in 2 μs by applying a square voltage of this duration to the laser head. This wavenumber sweep is repeated, typically at a frequency of 5 kHz, thereby enabling rapid acquisition of infrared spectra with good signal-to-noise ratio by averaging many successively acquired spectra. The linearly polarized, unfocused laser output was attenuated by using a rotatable linear polarizer (to avoid saturating the detector), and aligned along the viewing axis by using two 90° turning mirrors. The transmitted light was focused onto a liquid nitrogen cooled detector (Kolmar Technologies KV104-0.1-1A-3) with a parabolic mirror, and the detector output passed through a fast amplifier (Femto Messtechnik HAS-Y-1-40) to a fast data collection card (Acqiris DP210) in a PC running under Labview control. Spectra were transformed and linearized from time to wavenumber space by periodically measuring the interference fringes produced by inserting a Ge Etalon (free spectral range $= 0.0481$ cm^{-1}) into the laser beam path.

Results

By way of orientation, Figure 1 shows measured single pass, line-of-sight absorption spectra of MW activated 4.4% C_2H_2/7% Ar in H_2 (upper panel) and 8.8% CH_4/7% Ar in H_2 (lower panel) gas mixtures. The carbon mole fraction in each case is thus the same, as is the total flow rate (565 standard cm^3 per minute (sccm)), pressure (150 Torr), and applied MW power (1.5 kW). The same spectral features are evident in both spectra, but their relative intensities show significant variations. The displayed wavenumber range includes four strong absorption lines of the ν_4 band of CH_4 and two strong lines of the $\nu_4 + \nu_5$ combination band of C_2H_2. Several other absorption lines attributable to vibrationally excited C_2H_2 molecules with $\nu_4 = 1$ or $\nu_5 = 1$ are also evident.[25] The vibrational origins of these two levels lie respectively 614.0 and 731.5 cm^{-1} above the vibrational ground state.[25] Absolute wavenumbers for the C_2H_2 transitions were determined by fitting against literature values for the four CH_4 transitions.[26] This served to validate the C_2H_2

TABLE 1: Assignments of Observed C_2H_2 and CH_4 Absorption Lines

CH_4		
wavenumber/ cm^{-1} (ref 26)	vibrational transition	rotational transition
1277.47335	4_0^1	$4F_2-5F_1,1$
1276.84431	4_0^1	$4F_1-5F_2,1$
1275.38678	4_0^1	4E−5E
1275.04168	4_0^1	$4F_2-5F_1,2$

C_2H_2			
obsd wavenumber/cm^{-1}	lit. value/ cm^{-1} (ref 25)	vibrational transition	rotational transition[a]
1276.7807	1276.79005	$4_0^1 5_1^2(\Pi_g-\Pi_u)$	P(18, *e*)
1276.3284	1276.33656	$4_1^2 5_0^1(\Pi_u-\Pi_g)$	P(23, *f*)
1275.9443	1275.95852	$4_0^1 5_1^2(\Pi_g-\Pi_u)$	P(19, *f*)
1275.5006	1275.51215	$4_0^1 5_0^1(\Sigma_u^+-\Sigma_g^+)$	P(23)
1275.3725	1275.37459	$4_1^2 5_0^1(\Pi_u-\Pi_g)$	P(23, *e*)
1274.4764	1274.47943	$4_0^1 5_1^2(\Pi_g-\Pi_u)$	P(19, *e*)
1274.1521	1274.15632	$4_1^2 5_0^1(\Pi_u-\Pi_g)$	P(24, *f*)
1273.8193	1273.81965	$4_0^1 5_1^2(\Pi_g-\Pi_u)$	P(20, *f*)
1273.2646	1273.26188	$4_0^1 5_0^1(\Sigma_u^+-\Sigma_g^+)$	P(24)
1273.1024	1273.10380	$4_1^2 5_0^1(\Pi_u-\Pi_g)$	P(24, *e*)

[a] *e* and *f* indicate the *l*-type doubling components of the Π vibrational states.

and CH_4 line assignments indicated in Figure 1 (on the upper and lower spectra, respectively) and detailed in Table 1. No absorptions associated with vibrationally excited CH_4 molecules have been identified under the prevailing conditions, though CH_4 hot-band absorptions have been observed in this wavenumber region in long path length absorption measurements of other environments.[27]

The remainder of this paper serves to illustrate some of the opportunities afforded by this new, sensitive, nonintrusive, optical diagnostic method. As we show, the rapid sweep facility enables essentially simultaneous monitoring of the dominant hydrocarbons (CH_4 and C_2H_2) in these activated gas mixtures—as a function of process conditions (source gas, gas mixing ratios, chamber pressure, applied MW power, etc.)—and can provide insight into the time-dependence of interconversion between CH_4 and C_2H_2. However, this is a line-of-sight technique. It returns absorbances of the various target species in the particular quantum states probed. Inverting such measurements into (nonquantum state resolved) column densities of a chosen target molecule, or position dependent species number densities, requires detailed knowledge of the gas composition and the temperature distribution along the viewing column. Without detailed modeling of the local gas-phase chemistry, the flow fields, stagnation volumes, etc. within the present reactor, the very evident differences between the spectra recorded with the same input carbon mole fraction but different hydrocarbon process gases (Figure 1) do not necessarily contradict the view that the gas phase composition immediately adjacent to the growing diamond surface (and the details of ensuing microcrystalline diamond film growth) depends only on the local C:H ratios, and not the specific chemical identities of the feedstock gases.

From hereon we focus attention on the smaller wavenumber region between 1276.2 and 1274.6 cm^{-1}. Panels a and b of Figure 2 show absorption spectra measured over this range for three different $CH_4/Ar/H_2$ and $C_2H_2/Ar/H_2$ gas mixtures, chosen so as to allow comparison between samples containing input carbon fractions of 1%, 4.4%, and 8.8%. Ar constituted 7% of the total gas flow in each case, with H_2 making up the balance. The plasma composition was left to equilibrate for at least 5 min after each change in gas mixing ratio prior to recording the various spectra shown in this figure. Recalling Table 1, the discussion that follows focuses attention on the relative behaviors of the three spectral lines with wavenumbers of (literature values) 1275.9585 cm^{-1} (due to vibrationally excited C_2H_2-(υ_5=1) molecules (henceforth indicated simply as $C_2H_2^{\ddagger}$)), 1275.5122 cm^{-1} (associated with ground (υ = 0) state C_2H_2 molecules), and 1275.0417 cm^{-1} (due to ground-state CH_4 molecules). Interpreting the intensity of the fourth line, centered at ~1275.38 cm^{-1}, is less clear-cut as it includes contributions from overlapping $CH_4(\upsilon$=0) and $C_2H_2(\upsilon_4$= 1) absorptions. Panels c and d in Figure 2 show how the measured absorbances of the selected lines vary as a function of percent C in the input gas mixture, for both CH_4 and C_2H_2 source gases. Several qualitative trends are immediately apparent: Most of the absorption measured at low (1%) input carbon fractions is attributable to CH_4, irrespective of the identity of the input hydrocarbon. The absorbance associated with $C_2H_2^{\ddagger}$ molecules under these conditions is actually greater than that due to ground-state C_2H_2 and, again, seemingly insensitive to the choice of hydrocarbon source gas. As percent C increases, however, differences between CH_4 and C_2H_2 input gas mixtures become apparent. Absorption due to $C_2H_2^{\ddagger}$ increases steadily with percent C in both cases, but much less steeply than does the absorption due to ground-state C_2H_2 molecules. The trend in CH_4 absorption with increasing percent C provides the clearest distinction between the two input gases. With CH_4 as the source gas, the CH_4 absorption rises steadily with increasing percent C (though less steeply than the C_2H_2 absorption), whereas with C_2H_2 as the hydrocarbon source, the CH_4 absorbance maximizes at ~2% input C, and gently declines as percent C is increased further.

Conversion of these measured integrated absorbances, *A*, into column densities of CH_4 and C_2H_2 is far from straightforward, as the viewing column in the present experiment spans very inhomogeneous distributions of species number densities and gas temperatures. Cavity ring down spectroscopy masurements of $C_2(a)$ radicals in the same reactor indicate gas temperatures of ~3500 K,[28] but such measurements are heavily biased toward the center of the plasma ball where the temperature and the radical concentrations are highest. In contrast, the highest densities of stable molecules such as CH_4 and C_2H_2 will be in the coolest regions of the reactor. The HITRAN database[26] lists temperature-dependent line intensities, $S(T)$ (in units of cm^{-1}/(molecule cm^{-2})), for individual rovibrational transitions within both the 4_0^1 band of CH_4 and the $4_0^1 5_0^1$ combination band of C_2H_2. *S* provides a measure of the absorption intensity per molecule of the target species; its *T* dependence arises via the Boltzmann factor and the vibrational and rotational partition functions. Given a sample in thermal equilibrium at temperature *T*, the column density of the species of interest can be obtained simply by dividing the measured absorbance by the appropriate $S(T)$ value.

Unfortunately, when the plasma is running, the probed column spans inhomogeneous distributions of species number densities and local gas temperatures and, as Figure 3 shows, the *S* values for the P(23) line of the C_2H_2 $4_0^1 5_0^1$ band at 1275.5122 cm^{-1} and for the $4F_2-5F_1,2$ transition of the CH_4 4_0^1 band at 1275.0417 cm^{-1} monitored in this study show markedly different temperature dependences. $S(CH_4)$ is ~1.7× larger than $S(C_2H_2)$ at room temperature, but is some 5× smaller than $S(C_2H_2)$ at the highest gas temperatures relevant to the present reactor. Quantitative conversion of measured absorbances into column densities is thus not possible, and detailed concentration

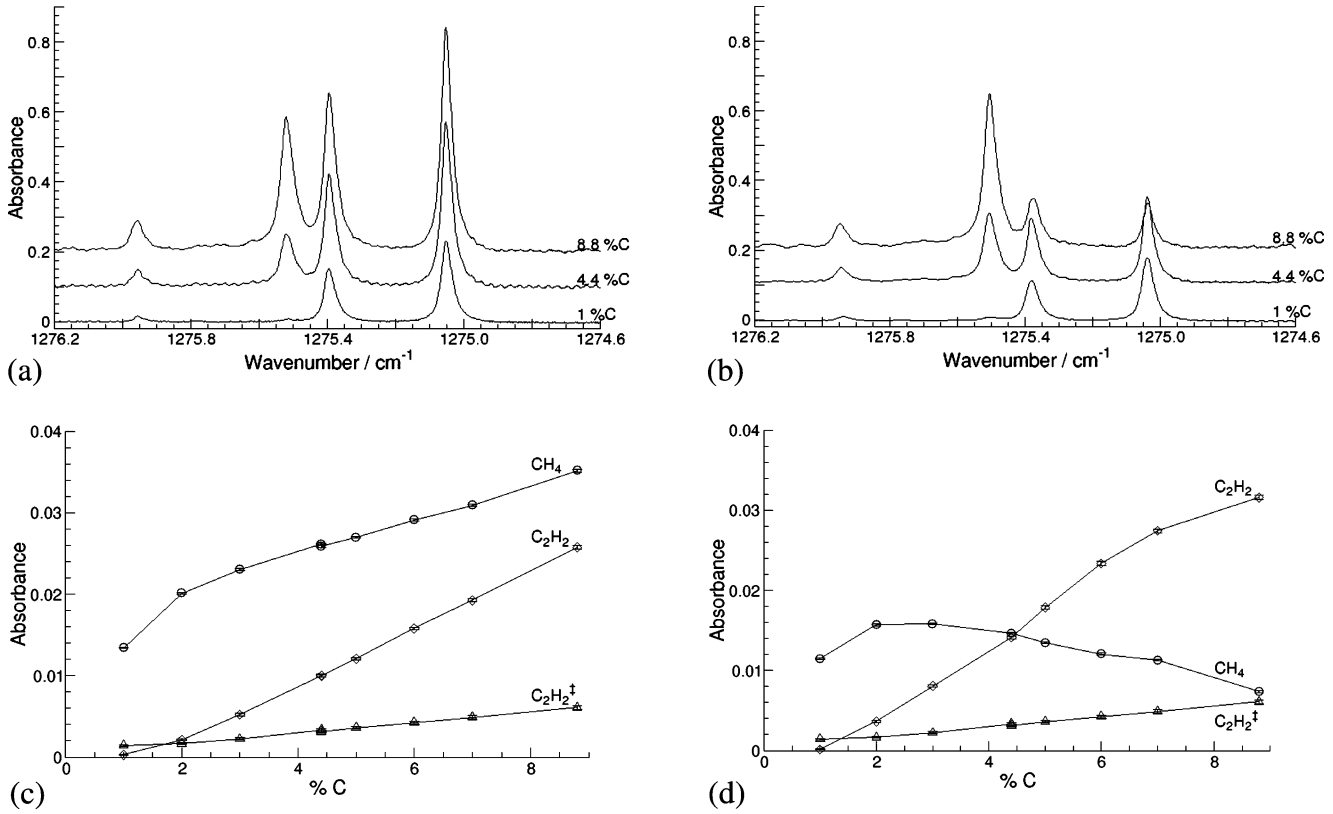

Figure 2. Absorption spectra measured over the range 1276.2−1274.6 cm^{-1} for (a) $CH_4/Ar/H_2$ and (b) $C_2H_2/Ar/H_2$ gas mixtures containing respectively C input fractions of 1%, 4.4%, and 8.8%. The respective spectra have been offset vertically, by 0.1 absorbance unit, for clarity. Plots c and d show how the absorbances of the 1275.9585 (due to $C_2H_2^{\ddagger}$), 1275.5122 (C_2H_2), and 1275.0417 cm^{-1} (CH_4) lines vary with percent C in the input gas mixture when using respectively $CH_4/Ar/H_2$ and $C_2H_2/Ar/H_2$ input gas mixtures.

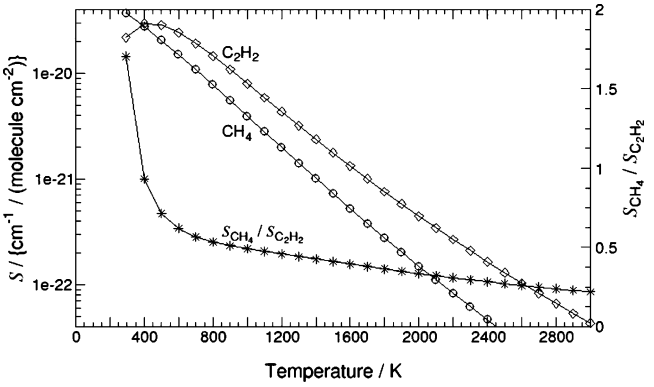

Figure 3. Semilogarithmic plot showing the temperature dependence of *S*, the intensity per molecule in units of $cm^{-1}/(molecule\ cm^{-2})$ when probing C_2H_2 (◇) via the P(23) line of the $4_0^1 5_0^1$ band at 1275.5122 cm^{-1} and CH_4 (○) by the $4F_2-5F_1$,2 transition of the 4_0^1 band at 1275.0417 cm^{-1} (left-hand axis). Also shown is the ratio of the respective $S(T)$ values (∗), plotted on a linear scale (right-hand axis).

profiling must await comparison with detailed reactor modeling calculations. Several qualitative conclusions can be drawn, however. Inspection of Figure 2d shows that C_2H_2 is the dominant absorber in the probed column within the activated 4.4% C_2H_2/7% Ar/H_2 gas mixture. Neglecting non-C_2H_2 contributions to the total carbon balance, mass dependent thermal diffusion effects, etc., the measured integrated absorbance ($A \sim 0.031$) can be reproduced assuming ideal gas behavior and a (not implausible) "effective" gas temperature of ∼700 K. The $S(CH_4)/S(C_2H_2)$ ratio at this temperature is ∼0.57. If we assume that the spatial distributions for CH_4 and C_2H_2 along the viewing column are broadly similar, we can get a feel for the relative column densities of CH_4 and C_2H_2 by roughly doubling the vertical scale for the CH_4 data in panels c and d of Figure 2. Thus we conclude that the CH_4 column density exceeds that of C_2H_2 not just for all $CH_4/Ar/H_2$ input gas mixtures investigated here, but also for all $C_2H_2/Ar/H_2$ gas mixtures containing less than ∼6% C (i.e. <3% C_2H_2). Finally, we note that, at low percent C, the absorbance of the $C_2H_2^{\ddagger}$ hot band feature at 1275.9585 cm^{-1} is consistently larger than that of the $C_2H_2(v=0)$ feature at 1275.5122 cm^{-1}. These transitions both involve excitation of the $\nu_4 + \nu_5$ combination, and differ only in the identity of the starting level. The respective transition dipole moments are expected to be very similar. The former originates from a slightly lower rotational state ($J = 19$), so its Hönl−London line strength factor will be ∼0.83× that of the 1275.5122 cm^{-1} feature. This is a small difference compared with the difference in the displayed absorbance at low percent C. We recognize that the vibrationally excited C_2H_2 molecules are more likely to be found in the hotter regions of the probed column, but the weakness of the $C_2H_2(v=0)$ absorption when using 1% C input gas mixtures (see Figure 2) can only be accommodated by assuming an inverted (i.e. nonthermal) population distribution over the C_2H_2 vibrational states.

Figure 4 illustrates the sensitivity of this same spectral region to the total gas pressure, *P*. The three spectra displayed in each of panels a and b of Figure 4 were measured using, respectively, equilibrated $CH_4/Ar/H_2$ and $C_2H_2/Ar/H_2$ gas mixtures that both contained 4.4% input fraction C, 7% Ar with the balance H_2, and $P = 50$, 100, and 150 Torr. The features of interest are described well by Lorentzian line shapes, as illustrated by the sample fits shown in Figure 4c. This is understandable given the relative magnitudes of the instrumental, Doppler, and pressure broadening contributions to the total line shape under the prevailing experimental conditions. The intrinsic bandwidth

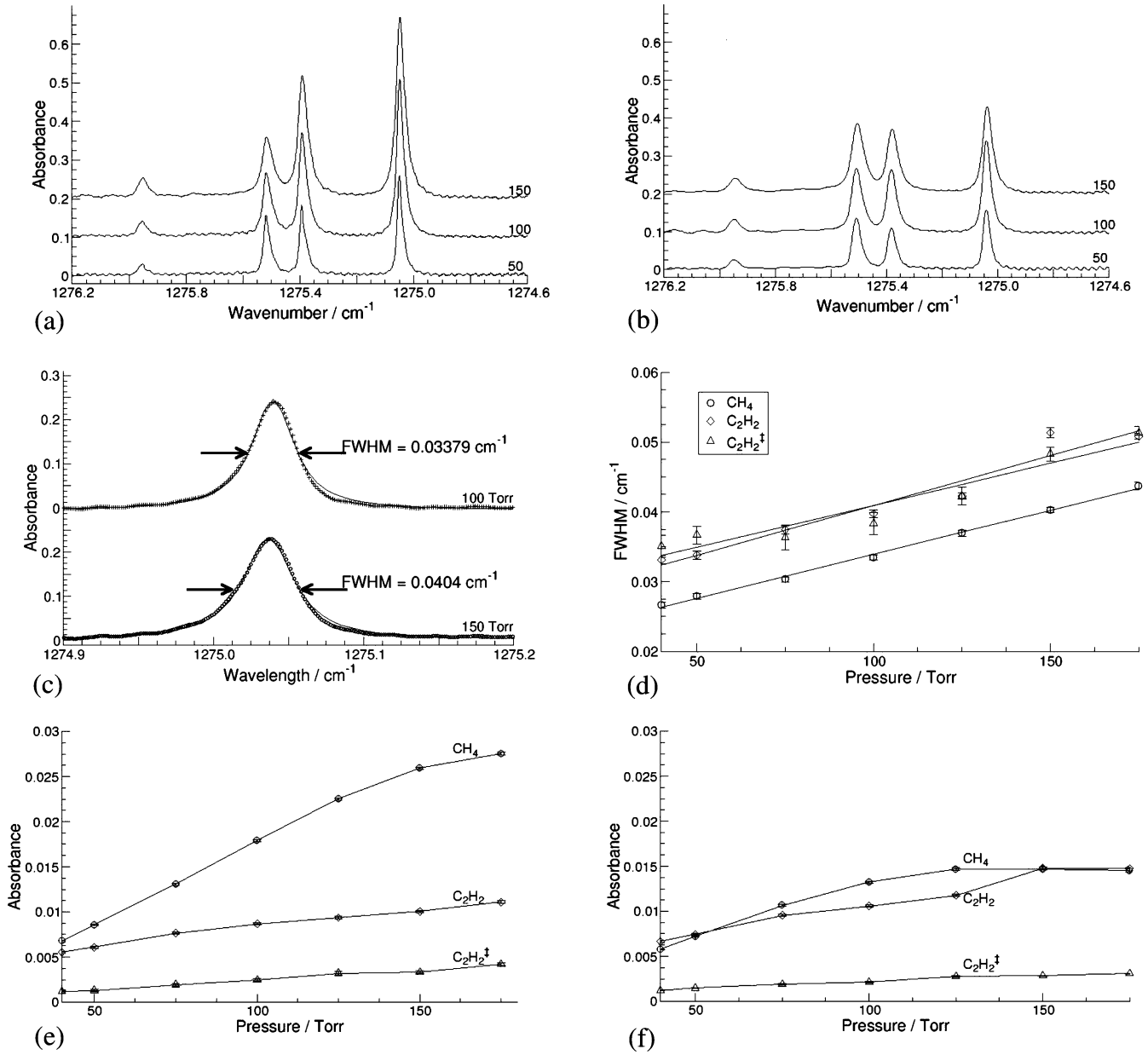

Figure 4. Absorption spectra measured over the range 1276.2−1274.6 cm^{-1} for (a) $CH_4/Ar/H_2$ and (b) $C_2H_2/Ar/H_2$ gas mixtures containing 4.4% C input fractions at total gas pressures of 50, 100, and 150 Torr (as indicated at the right-hand end of each spectrum). The respective spectra have each been offset vertically by 0.1 absorbance unit for ease of display. Panel c illustrates the quality of Lorentzian fits to the 1275.0417 cm^{-1} (CH_4) line shapes measured using the 2.2% $C_2H_2/Ar/H_2$ gas mixture at $P = 100$ and 150 Torr, while panel d shows the P dependence of the full width half-maximum (fwhm) values obtained by fitting the 1275.9585 ($C_2H_2^{\ddagger}$), 1275.5122 (C_2H_2), and 1275.0417 cm^{-1} (CH_4) line shapes in spectra obtained using the same mixing ratio as in panel c. The final two plots show the P dependence of the respective $C_2H_2^{\ddagger}$, C_2H_2, and CH_4 absorbances when using (e) 4.4% $CH_4/Ar/H_2$ and (f) 2.2% $C_2H_2/Ar/H_2$ input gas mixtures.

of the QC laser is of the order of 100 kHz, but the instrumental resolution is limited by the rate of change of the device temperature (and thus output frequency), ranging from ∼0.008 to ∼0.004 cm^{-1} (fwhm) during the 2 μs current pulse. Estimating the Doppler broadening contribution requires an "effective" value for the gas temperature, T_{gas}. For the purpose of this estimate we persist with an assumed $T_{gas} = 700$ K. Doppler broadening should thus give a (Gaussian) contribution to the width of a CH_4 line at ∼1275 cm^{-1} of ∼0.006 cm^{-1} (fwhm). The corresponding contribution to a C_2H_2 line would be ∼0.005 cm^{-1} (fwhm). Doppler and instrumental contributions are thus both small compared with the measured line widths of the CH_4 and C_2H_2 transitions, all of which increase with P as shown in Figure 4d. Pressure broadening coefficients, γ, derived from such data are of limited value given the (P dependent) variation in species (and total) number densities, and temperature, along the viewing column, but the gradient of the line width versus P plot for the CH_4 line, for example, equates to $\gamma \sim 3.9$ MHz/Torr. Note that the collision frequencies at the pressures used in the present experiments are sufficiently high to obviate line shape complications due to effects of rapid adiabatic passage, such as have been observed when using a frequency chirped QC laser to probe much lower pressure gas samples.[21] Panels e and f of Figure 4 show the pressure-dependent absorbances due to the $C_2H_2^{\ddagger}$, C_2H_2, and CH_4 features of interest. The total carbon content in these gas mixtures increases 3-fold as P is raised from 50 and 150 Torr. This increase is roughly mirrored by the CH_4 and $C_2H_2^{\ddagger}$ absorbances measured when using CH_4 as the input hydrocarbon, but the absorption associated with ground-state C_2H_2 molecules in-

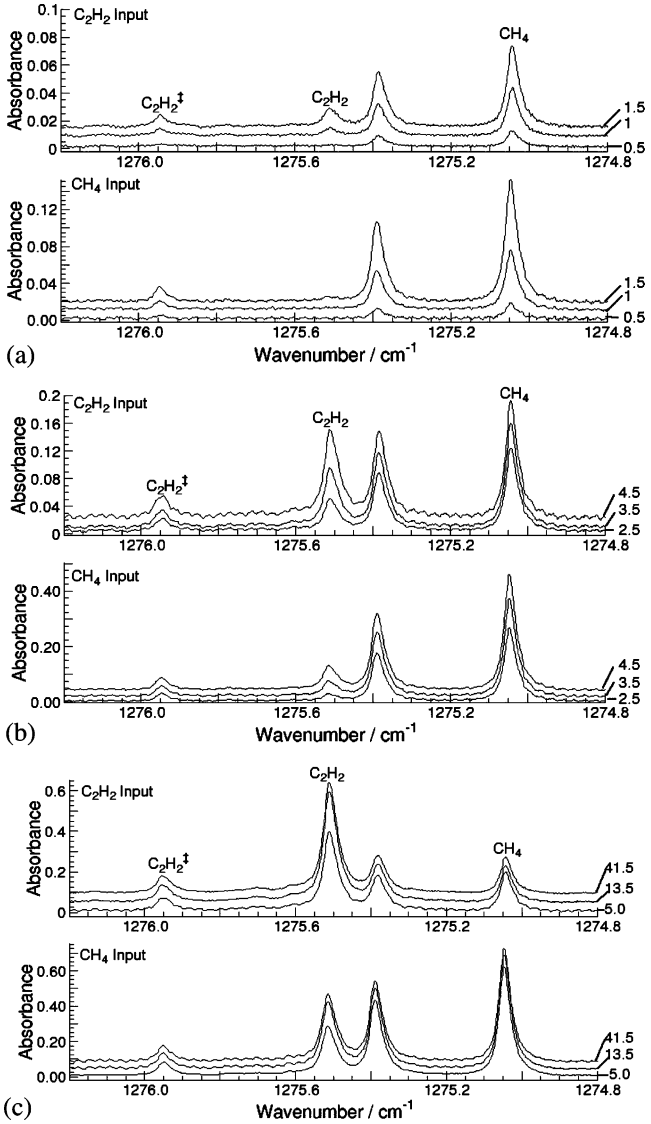

Figure 5. Absorption spectra measured over the range 1276.2−1274.6 cm^{-1}, as a function of time (in s, indicated at the right-hand end of each trace) following addition of 4.4% C_2H_2 (upper traces in each panel) and 8.8% CH_4 (lower traces) to a pre-established Ar/H_2 plasma. Spectra shown in panels a, b, and c were recorded at progressively later times after the instant of hydrocarbon addition to the mixing manifold, and the spectra displayed in any one panel have been offset vertically for display purposes.

creases less steeply. Somewhat different behavior is observed when C_2H_2 is the source hydrocarbon. In this case, the C_2H_2 and $C_2H_2^{\ddagger}$ absorbances increase with P, while the CH_4 absorption appears to plateau at $P \sim 100$ Torr. Again, detailed discussion of these observations, and their conversion to column densities, must await more detailed modeling of the temperature and species number density distributions within this reactor.

The rapid spectral acquisition rate achievable with a frequency chirped QC laser has also allowed investigation of the way the column density approaches equilibrium after introduction (or cessation) of the hydrocarbon flow into a pre-established 7% Ar in H_2 plasma. Illustrative data following introduction of 4.4% C_2H_2 (upper traces) and 8.8% CH_4 (lower traces) are given in each of the three panels displayed in Figure 5. The number appearing at the right-hand end of each trace indicates the time, t (in seconds), at which the spectrum was recorded following introduction of the hydrocarbon flow into the premixing manifold (at $t = 0$). Detailed interpretation of these observations

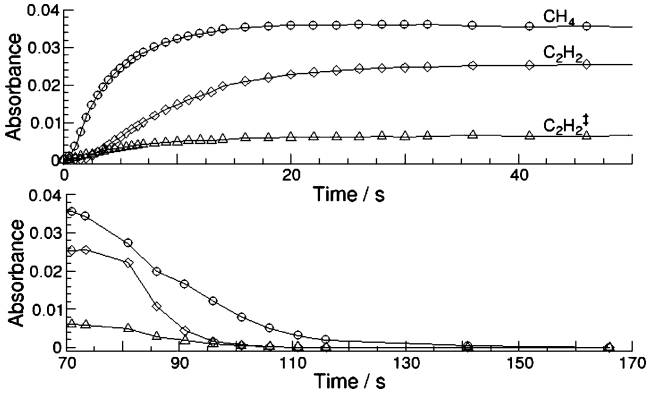

Figure 6. Plot showing variation of CH_4, C_2H_2, and $C_2H_2^{\ddagger}$ absorbances with time after the introduction (at $t = 0$ s) of 8.8% CH_4 to a pre-established 7% Ar in H_2 plasma and, below, the subsequent fall in these signals from their equilibrium values when the hydrocarbon feed is cut (at $t = 70$ s).

will also require more thorough modeling and understanding of the reactor flow fields and the distributions of species population and temperature along the probed column than is currently available but, once again, a number of striking and hitherto unreported trends are immediately apparent. No CH_4 or C_2H_2 signals are observed at $t < 0$, even when the substrate is covered by a pre-grown CVD diamond film, implying that etching processes make negligible contribution to the present absorption measurements and that these are sensitive solely to gas-phase chemistry. Even at the earliest time after opening the hydrocarbon MFC ($t = 0.5$ s), carbon has reached the probed column—but the dominant absorptions are those of CH_4, even when C_2H_2 is used as the source gas. Additionally, the absorption due to $C_2H_2^{\ddagger}$ is greater than that from ground-state C_2H_2. Recalling Figure 2, we note that such trends are very reminiscent of those observed under equilibrium conditions when using dilute (e.g. 1% C content) gas mixtures. With C_2H_2 as source gas, the absorption due to ground-state C_2H_2 molecules has overtaken that due to $C_2H_2^{\ddagger}$ by $t = 1.5$ s; when using CH_4, we require $t \sim 3.5$ s to achieve a C_2H_2 absorption greater than that from $C_2H_2^{\ddagger}$. Thereafter, in both cases, the CH_4 and $C_2H_2^{\ddagger}$ absorptions both reach their steady-state values faster than does the C_2H_2 absorption. Indeed, when using CH_4 as the source gas, the CH_4 absorption barely increases after $t = 5$ s. In both cases, the various line intensities in the spectra recorded at $t = 41.5$ s are in quantitative accord with those shown in Figure 1, validating our earlier assumption that equilibrium conditions are reached well within 5 min of any change in gas mixing ratio. These trends are summarized in Figure 6, which shows the measured t dependent rise in CH_4, C_2H_2, and $C_2H_2^{\ddagger}$ absorbances when 8.8% CH_4 is introduced to a pre-established 7% Ar in H_2 plasma, and the subsequent fall in these signals from their equilibrium values when the hydrocarbon feed is cut (at $t = 70$ s). Again, the CH_4 and $C_2H_2^{\ddagger}$ absorptions are seen to exhibit a qualitatively different time response to the change in hydrocarbon feed than does the C_2H_2 signal.

Discussion

This study provides the first illustration of the utility of pulsed QC lasers for in situ probing of the gas-phase chemistry prevailing in a 2 kW MW plasma enhanced reactor during diamond CVD. Specifically, both CH_4 and C_2H_2 molecules, and their interconversion, have been monitored as a function of process conditions (e.g., choice of input hydrocarbon (CH_4 or C_2H_2), hydrocarbon mole fraction, total gas pressure, and applied

MW power). The measured quantities are line-of-sight absorbances and, as pointed out previously, the conversion of such measurements into absolute column densities is hampered by the inhomogeneous species number density and temperature distributions along the viewing column. The absolute sensitivity achieved in these preliminary investigations could be much improved, by multipassing the probe beam and by more careful design and mounting of the windows (so as to obviate etaloning effects). Vertical profiling of the plasma ball will be trivial to implement.

Quantitative analysis of these (and related future) measurements will proceed in tandem with detailed modeling of the plasma chemical transformations and heat and mass transfer processes within these MW activated gas mixtures—as in our recent combined experimental and modeling studies of a diamond depositing DC arc jet reactor operating with CH_4/H_2/Ar gas mixtures.[17,29] Key, new findings from these preliminary studies are the very obvious preference for C to be present as CH_4 in the more dilute hydrocarbon gas mixtures, irrespective of the hydrocarbon source gas, the inverted C_2H_2 vibrational state population distribution when using low C fractions, and the progressive switch toward C_2H_2 as the input C fraction increases.

These trends are all understandable, qualitatively, within the framework of existing models of the gas-phase chemistry prevailing in activated hydrocarbon/H_2 mixtures under conditions appropriate for diamond CVD. As shown previously,[3,15,16] interconversion between CH_4 and C_2H_2 involves a multistep reaction sequence, the overall rate (and even the sign) of which is sensitively dependent upon the local hydrocarbon and H atom number densities, and the local gas temperature—all of which are reactor and process specific. Of particular relevance to the present observations was the finding that $C_2H_2 \rightarrow CH_4$ conversion can be driven by a sequence of (third body stabilized) H atom addition reactions at low ($<$1000 K) gas temperatures.[3,16] High H atom concentrations, and such comparatively low gas temperatures, are precisely the conditions that will be encountered at the top of the reactor when C_2H_2 is first introduced into a pre-existing Ar/H_2 plasma (recall Figure 5a). Similar trends were observed under steady-state conditions when using low input flow rates of C_2H_2 (recall Figure 2b). This can be understood also by recognizing that similar $C_2H_2 \rightarrow CH_4$ conversions will occur in regions distant from the plasma ball (e.g. at both ends of the viewing column) where, because the gas is cooler, most of the total number density will be concentrated.

Increasing the hydrocarbon input will increase the rates of reactions 1 and 2, and thus lead to a reduction in the H atom concentrations throughout the reactor. This, and the associated increase in CH_y radical concentrations, will both serve to shift the equilibrium back in favor of C_2H_2—as observed. The dominant showing of the respective source gases in spectra recorded at high (8.8%) C input ratios (Figure 2c) is most readily understandable by assuming that, in these cases, the hydrocarbon/H atom ratios are becoming large enough that a significant fraction of the input hydrocarbon flow escapes processing en route to the viewing column. Finally we address the observed trends in $C_2H_2^{\ddagger}$. $CH_4 \rightarrow C_2H_x$ interconversion occurs via the H-shifting reactions 1 and 2; C_2H_2 ($x = 2$) is the more stable species at high T, so this interconversion will occur preferentially in the hottest regions of the reactor. However, we have argued that the $C_2H_2^{\ddagger}$ and $C_2H_2(v=0)$ absorbances should be fairly reliable indicators of their respective column densities and that the $C_2H_2^{\ddagger}$ column density actually exceeds that of $C_2H_2(v=0)$ in dilute hydrocarbon/H_2 mixtures. Possible reasons for this deduced population inversion are not hard to find. The last step in the kinetic scheme driving $CH_4 \rightarrow C_2H_2$ in hot regions of the reactor involves the conversion $C_2H_3 + H \rightleftharpoons C_2H_2 + H_2$. This reaction is fast,[30] and exothermic by $\sim$290 kJ mol^{-1}.[31] The present measurements suggest that at least some of this reaction exoergicity is channeled into vibrational excitation of the nascent C_2H_2 products—and probably into many excited vibrational levels additional to the $v_5 = 1$ level probed in this work. That being so, diagnostic methods that sample just $C_2H_2(v=0)$ molecules may yield serious underestimates of the total C_2H_2 column (or number) density in situations where the rate of C_2H_2 production via reaction 2 significantly exceeds the vibrational relaxation (and thermal equilibration) rates of the resulting $C_2H_2^{\ddagger}$ species.

Acknowledgment. The Bristol group are grateful to EPSRC for the award of a portfolio grant (LASER) and postdoctoral support via the Carbon Based Electronics initiative (J.A.S.), to Element Six Ltd for the long term loan of the MW reactor and for the award of an Industrial CASE studentship (A.C.), to Dr. Yu. A. Mankelevich (Moscow State University) for his huge contributions to our understanding of the gas phase chemistry underpinning diamond CVD processes, and to colleagues E. Crichton, P. Fiadzomor, K. N. Rosser, and Dr. C. M. Western for their many and varied contributions to the work described herein. The Strathclyde group are indebted to NERC for the award of a COSMAS grant and for a studentship (S.W.) and to AWE Aldermaston for their support for the development of the QC laser spectrometer.

References and Notes

(1) Celii, F. G.; Butler, J. E. *Annu. Rev. Phys. Chem.* **1991**, *42*, 643.
(2) Goodwin, D. G.; Butler, J. E. In *Handbook of Industrial Diamonds and Diamond Films*; Prelas, M. A., Popovici, G., Bigelow, L. G., Eds.; Marcel Dekker: New York, 1998; pp 527−81 and references therein.
(3) Ashfold, M. N. R.; May, P. W.; Petherbridge, J. R.; Rosser, K. N.; Smith, J. A.; Mankelevich, Y. A.; Suetin, N. V. *Phys. Chem. Chem. Phys.* **2001**, *3*, 3471 and references therein.
(4) Hsu, W. L.; McMaster, M. C.; Coltrin, M. E.; Dandy, D. S. *Jpn. J. Appl. Phys.* **1994**, *33*, 2231.
(5) Rego, C. A.; May, P. W.; Henderson, C. R.; Ashfold, M. N. R.; Rosser, K. N.; Everitt, N. M. *Diamonds Relat. Mater.* **1995**, *4*, 770.
(6) Celii, F. G.; Pehrsson, P. E.; Wang, H.-t.; Butler, J. E. *Appl. Phys. Lett.* **1988**, *52*, 2043.
(7) Luque, J.; Juchmann, W.; Jeffries, J. B. *J. Appl. Phys.* **1997**, *82*, 2072.
(8) Wahl, E. H.; Owano, T. G.; Kruger, C. H.; Zalicki, P.; Ma, Y.; Zare, R. N. *Diamonds Relat. Mater.* **1996**, *5*, 373.
(9) Cappelli, M. A.; Owano, T. G.; Gicquel, A.; Duten, X. *Plasma Chem. Plasma Proc.* **2000**, *20*, 1.
(10) See, for example: Wills, J. B.; Smith, J. A.; Boxford, W. E.; Elks, J. M. F.; Ashfold, M. N. R.; Orr-Ewing, A. J. *J. Appl. Phys.* **2002** *92*, 4213.
(11) John, P.; Rabeau, J.; Wilson, J. I. B. *Diamonds Relat. Mater.* **2002**, *11*, 608.
(12) Meier, U.; Kohse-Hoinghaus, K.; Schafer, L.; Klages, C.-P. *Appl. Opt.* **1990**, *29*, 4993.
(13) Gicquel, A.; Chenevier, M.; Breton, Y.; Petiau, M.; Booth, J. P.; Hassouni, K. *J. Phys. III* **1996**, *6*, 1167.
(14) Redman, S. A.; Chung, C.; Rosser, K. N.; Ashfold, M. N. R. *Phys. Chem. Chem. Phys.* **1999**, *1*, 1415.
(15) Smith, J. A.; Cameron, E.; Ashfold, M. N. R.; Yu. Mankelevich, A.; Suetin, N. V. *Diamonds. Relat. Mater.* **2001**, *10*, 358.
(16) Mankelevich, Yu. A.; Suetin, N. V.; Ashfold, M. N. R.; Smith, J. A.; Cameron, E. *Diamonds Relat. Mater.* **2001**, *10*, 364.
(17) Rennick, C. J.; Smith, A. G.; Smith, J. A.; Wills, J. B.; Orr-Ewing, A. J.; Ashfold, M. N. R.; Mankelevich, Yu. A.; Suetin, N. V. *Diamonds Relat. Mater.* **2004**, *13*, 561.
(18) Bachmann, P. K.; Leers, D.; Lydtin, H. *Diamonds Relat. Mater.* **1991**, *1*, 1 and references therein.
(19) Kazarinov, R. F.; Suris, R. A. *Sov. Phys. Semicond.* **1971**, *5*, 707.
(20) Faist, J.; Capasso, F.; Sivco, D. L.; Sirtori, C.; Hutchinson, A. L.; Cho, A. Y. *Science* **1994**, *264*, 553.

(21) Duxbury, G.; Langford, N.; McCulloch, M. T.; Wright, S. *Chem. Soc. Rev.* **2005**, *34*, 1.

(22) McCulloch, M. T.; Normand, E. L.; Langford, N.; Duxbury, G.; Newnham, D. A. *J. Opt. Soc. Am. A* **2003**, *20*, 1761.

(23) McCulloch, M. T.; Langford, N.; Duxbury, G. *Appl. Opt.* **2005**, *44*, 2887.

(24) Cascade Technolgies Ltd., 141 St James Road, Glasgow G4 0LT.

(25) Kabbadi, Y.; Herman, M.; di Lonardo, G.; Fusina, L.; Johns, J. W. C. *J. Mol. Spectrosc*. **1991**, *150*, 535.

(26) HITRAN 2000. Rothman, L. S.; Barbe, A.; Benner, D. C.; Brown, L. R.; Camy-Peyret, C.; Carleer, M. R.; Chance, K.; Clerbaux, C.; Dana, V.; Devi, V. M.; Fayt, A.; Flaud, J.-M.; Gamache, R. R.; Goldman, A.; Jacquemart, D.; Jucks, K. W.; Lafferty, W. J.; Mandin, J.-Y.; Massie, S. T.; Nemtchinov, V.; Newnham, D. A.; Perrin, A.; Rinsland, C. P.; Schroeder, J.; Smith, K. M.; Smith, M. A. H.; Tang, K.; Toth, R. A.; Vander Auwera, J.; Varanasi, P.; Yoshino, K. *J. Quant. Spectrosc. Radiat. Transfer* **2003**, *82*, 5.

(27) McCulloch, M. T.; Wright, S.; Langford, N.; Duxbury, G. Unpublished results.

(28) Cheesman, A.; Smith, J. A.; Ma, J.; Henney, J. J.; Coulson, B. R.; Ashfold, M. N. R. Unpublished results.

(29) Rennick, C. J.; Engeln, R.; Smith, J. A.; Orr-Ewing, A. J.; Ashfold, M. N. R.; Mankelevich, Yu. A. *J. Appl. Phys*. **2005**, *97*, 113306.

(30) Baulch, D. L.; Cobos, C. J.; Cox, R. A.; Esser, C.; Frank, P.; Just, Th.; Kerr, J. A.; Pilling, M. J.; Troe, J.; Walker, R. W.; Warnatz, J. *J. Phys. Chem. Ref. Data* **1992**, *21*, 411 and references therein.

(31) http://webbook.nist.gov/chemistry/.